Preclinical Development

Molecular Cancer Therapeutics

Ridaforolimus (AP23573; MK-8669), a Potent mTOR Inhibitor, Has Broad Antitumor Activity and Can Be Optimally Administered Using Intermittent Dosing Regimens

Victor M. Rivera, Rachel M. Squillace, David Miller, Lori Berk, Scott D. Wardwell, Yaoyu Ning, Roy Pollock, Narayana I. Narasimhan, John D. Iuliucci, Frank Wang, and Tim Clackson

Abstract

The mTOR pathway is hyperactivated through oncogenic transformation in many human malignancies. Ridaforolimus (AP23573; MK-8669) is a novel rapamycin analogue that selectively targets mTOR and is currently under clinical evaluation. In this study, we investigated the mechanistic basis for the antitumor activity of ridaforolimus in a range of human tumor types, exploring potential markers of response, and determining optimal dosing regimens to guide clinical studies. Administration of ridaforolimus to tumor cells *in vitro* elicited dose-dependent inhibition of mTOR activity with concomitant effects on cell growth and division. We showed that ridaforolimus exhibits a predominantly cytostatic mode of action, consistent with the findings for other mTOR inhibitors. Potent inhibitory effects on vascular endothelial growth factor secretion, endothelial cell growth, and glucose metabolism were also observed. Although PTEN and/or phosphorylated AKT status have been proposed as potential mTOR pathway biomarkers, neither was predictive for ridaforolimus responsiveness in the heterogeneous panel of cancer cell lines examined. In mouse models, robust antitumor activity was observed in human tumor xenografts using a series of intermittent dosing schedules, consistent with pharmacodynamic observations of mTOR pathway inhibition for at least 72 hours following dosing. Parallel skin-graft rejection studies established that intermittent dosing schedules lack the immunosuppressive effects seen with daily dosing. Overall these findings show the broad inhibitory effects of ridaforolimus on cell growth, division, metabolism, and angiogenesis, and support the use of intermittent dosing as a means to optimize antitumor activity while minimizing systemic effects. *Mol Cancer Ther; 10(6); 1059–71. ©2011 AACR.*

Introduction

mTOR is a highly conserved serine/threonine kinase that acts as a central regulator of cell growth and division, integrating cellular cues in response to nutritional and environmental conditions (1–3). In this role, mTOR functions as a sensor of nutrient, mitogen, and energy levels, and serves as a 'gatekeeper' for the G_1- to S-phase transition of the cell cycle (2). The prototypic mTOR inhibitor, the natural product macrolide rapamycin, was initially characterized as having antifungal activity, but subsequently determined to have broad antiproliferative and cytostatic activity against eukaryotic cells (4). Due to particularly potent activity against activated T cells, a daily dosing regimen of rapamycin (Rapamune) was approved for the prevention of allograft rejection following organ transplantation.

Early work evaluating the immunosuppressive activity of rapamycin also showed antitumor activity, leading to the identification of mTOR as a potential target for cancer therapy. Signaling pathways that impinge on mTOR activity, most prominently the PI3K/AKT axis, are commonly dysregulated during tumorigenesis, suggesting that mTOR signaling contributes to maintenance of a transformed phenotype (2, 3). Accordingly, hyperactivation of PI3K/AKT signaling is linked to critical aspects of tumor cell biology, including resistance to apoptosis, increased cell proliferation, and metabolism (5–7). Aberrant activation of this pathway can occur through functional loss of the PTEN tumor suppressor, mutations of which occur with high frequency in human malignancies. Indeed, it has been reported that tumors that harbor defects in PTEN function can be hypersensitive to inhibition of mTOR in preclinical studies (8, 9). AKT also modulates mTOR signaling through the activity of another tumor suppressor, the tuberous sclerosis complex

Authors' Affiliation: ARIAD Pharmaceuticals, Inc., Cambridge, Massachusetts

Note: Supplementary material for this article is available at Molecular Cancer Therapeutics Online (http://mct.aacrjournals.org/).

V.M. Rivera and R.M. Squillace contributed equally to this work.

Corresponding Author: Victor M. Rivera, ARIAD Pharmaceuticals, Inc., 26 Landsdowne Street, Cambridge, MA 02139. Phone: 617-494-0400; Fax: 617-494-8144. E-mail: victor.rivera@ariad.com

doi: 10.1158/1535-7163.MCT-10-0792

(TSC; ref. 10). This complex is a heterodimer of 2 proteins, TSC1 and TSC2, which serves as a negative upstream regulator of mTOR activity (11). Mutations in these genes result in the tumor-prone syndrome tuberous sclerosis.

Constitutive mTOR signaling contributes to malignant transformation, at least in part, through promotion of cell-cycle progression. mTOR controls protein synthesis through the activation of S6 kinase (S6K1) and its substrate ribosomal protein S6, and through the inactivation of the repressor of mRNA translation, eukaryotic initiation factor 4E-binding protein (4E-BP1). By regulating translation of proteins critical for exit from the G_1 phase of the cell cycle, such as cyclin D1 (12, 13), and by stimulating mislocalization and elimination of the cyclin-dependent kinase inhibitor $p27^{kip1}$ (14), mTOR plays a key role in regulating progression through the cell cycle and therefore cell proliferation. Although blockade of the mTOR pathway leads to apoptosis in some instances (15, 16), a cytostatic effect is more generally observed (17, 18). Further, elevated mTOR activity provides tumors with additional selective advantages. As a cellular nutrient sensor, mTOR signaling promotes glucose utilization via increased expression and activity of the glucose transporter GLUT1 (19, 20). In addition, mTOR is a known regulator of HIF-1α expression and activity (19), which in turn controls expression of vascular endothelial growth factor (VEGF), a factor important for tumor vascularization (21, 22), and by stimulating VEGF-dependent proliferation of endothelial cells (23). Therefore, inhibition of mTOR function can exert antitumorigenic effects through multiple mechanisms that impact cell growth, division, metabolism, and angiogenesis. In this regard, treatment of tumor cells with rapamycin inhibits all of these processes and induces a phenotype that resembles that seen with nutrient starvation (24).

Collectively, these observations identify mTOR as an attractive molecular target for therapeutic intervention in human cancer. As a consequence, analogues of rapamycin have emerged as a class of drugs currently being developed for their antineoplastic properties (25). Ridaforolimus (AP23573; MK-8669) is a novel nonprodrug analogue of rapamycin, designed to inhibit the growth and proliferation of tumor cells by inhibiting the activity of the mTOR protein (26). In early clinical trials, this agent has shown antitumor activity against a variety of human cancers (27, 28). The overall goal of the present study was to explore the *in vitro* and *in vivo* pharmacology of ridaforolimus to guide ongoing clinical development. A series of studies were conducted to dissect the mechanism of action of the compound and to evaluate the antiproliferative and antitumor activity across a range of cancer types. In addition, we explored potential molecular correlates of ridaforolimus sensitivity *in vitro*, consistent with the aim of identifying patients who might respond best to therapy. Finally, we explored the efficacy of the compound in mouse models, including an exploration of intermittent dosing schedules as a means to optimize the antitumor potency of the compound while minimizing systemic effects.

Materials and Methods

Antibodies and reagents

Ridaforolimus (AP23573; MK-8669; Supplementary Fig. S1) was synthesized at ARIAD Pharmaceuticals. A 1 mmol/L stock solution of ridaforolimus in ethanol was prepared and was diluted in the appropriate cell culture medium for *in vitro* cellular assays. For *in vivo* studies, ridaforolimus was diluted in a vehicle of 4% ethanol, 5% Tween 80, and 5% propylene glycol. Antibodies used were all rabbit polyclonals and included phospho-S6 ribosomal protein (Ser235/236) and phospho-AKT (Ser473) from Cell Signaling Technology; phospho-4E-BP1 (Ser65/Thr70) from Santa Cruz Biotechnology; GLUT1 and GAPDH (glyceraldehyde-3-phosphate dehydrogenase) from Abcam; GLUT4 from Millipore; and HIF-1α from BD Biosciences. The PTEN status of cell lines was determined by immunoblotting with a PTEN antibody (Cell Signaling Technology). The results were in agreement with those reported by the Cancer Genome Project (Wellcome Trust Sanger Institute, UK; http://www.sanger.ac.uk/genetics/CGP).

Cell culture

The following human tumor lines were obtained from the American Type Culture Collection (ATCC): HCT-116, SK-UT-1, HT-1080, SW872, MCF7, SK-LMS-1, U-87, A-204, PC-3, and SK-UT-1B. The TRI102 (#PTA-7368) and TRI103 (#PTA-7369) were obtained from the patent deposit, ATCC. Endothelial cells [human umbilical vein endothelial cells (HUVEC)] were obtained from Cell Applications, Inc. Cells were maintained and cultured according to standard techniques at 37°C in 5% (v/v) CO_2 using culture medium recommended by the supplier. All ATCC cell lines were authenticated by the company routine Cell Biology Program and were used within 6 months of receipt for this study. No authentication of the HUVEC line was done by our authors.

Flow cytometric analysis

HT-1080 (human fibrosarcoma) cells cultured in 10-cm dishes were treated for 24 hours with 100 nmol/L ridaforolimus, vehicle, or media alone (no treatment). The cells were then harvested and fixed with 70% ethanol/30% PBS overnight at 4°C. Fixed cells were washed and then sequentially incubated with 50 μg/mL RNase A (37°C for 30 minutes) and 20 μg/mL propidium iodide (room temperature for 30 minutes in the dark). DNA content was assessed using a FACSort flow cytometer and CELLQuest V3.1 software (Becton Dickinson). The percentage of cells in each phase of the cell cycle was estimated from the FL2-A channel data using ModFit LT for Mac V2.0 software (Verity Software House, Inc.). For cell size analysis, HT-1080 cells were incubated for 72 hours in the presence or absence of ridaforolimus at a

concentration of 100 nmol/L. Cells were harvested, fixed in 70% ethanol, and analyzed on a FACSort flow cytometer. Cell size was monitored by measuring the mean forward scatter height (FSC-H). Forward scatter is proportional to cell surface area and provides a measure of relative cell size. Mean FSC-H values were obtained from FSC-H histograms.

Glucose uptake assay and GLUT1 surface expression

Exponentially growing HT-1080 cells were treated with 100, 10, 1, 0.1 and 0.01 nmol/L ridaforolimus or vehicle. Cells were incubated for 48 hours before trypsinization and harvesting for glucose uptake and GLUT1 surface expression analysis. For glucose uptake, cells were stained with buffer containing 15% FBS, 0.25 mmol/L 2-deoxyglucose (2-DG), and 10 μmol/L 2-(*N*-(7-nitrobenz-2-oxa-1,3-diazol-4-yl)amino)-2-deoxyglucose (2-NBDG) for 2 hours at 37°C, and protected from light. After staining, cells were passed through a 30 μm mesh filter, maintained in the dark on ice, and analyzed immediately by flow cytometry. For the GLUT1 ligand binding assay, 10^5 cells were incubated in PBS containing 2% FBS and a 1:25 stock dilution of enhanced green fluorescent protein conjugated GLUT1 ligand (AbCys S.A.) for 30 minutes at 37°C, and protected from light. Cells were washed, maintained on ice in the dark, and analyzed immediately by flow cytometry. Glucose uptake levels and GLUT1 ligand binding were each determined by fluorescence-activated cell sorting (FACS) analysis using a FACSort flow cytometer and CellQuest Software. Intact single cells (1×10^4) were collected and the geometric mean FL-1 fluorescence was measured by the CELLQuest software. The relative percent glucose uptake or GLUT1 surface expression for each sample was then calculated using the formula: relative percentage (%) = (sample geometric mean fluorescence/vehicle treated geometric mean fluorescence) × 100. The relative glucose uptake and GLUT1 surface expression (%) values for the HT-1080 cells ± ridaforolimus are presented.

Immunoblotting

HT-1080 cells were treated with increasing concentrations of ridaforolimus (0–100 nmol/L) for 2 hours. To measure glucose transporter expression, HT-1080 cells were cultured in the presence or absence of 100 nmol/L ridaforolimus for 72 hours. In separate experiments, PC-3, U87, SK-LMS-1, SW872, HT-1080, SK-UT-1, and HCT116 cells were treated with a single 100 nmol/L dose of ridaforolimus for 2 and 24 hours before cell harvest. Cellular lysates were extracted in denaturing lysis buffer, resolved on SDS-PAGE and transferred to PVDF membranes. After blocking, membranes were incubated with primary antibodies for 1 hour, followed by appropriate horseradish peroxidase-conjugated secondary antibodies for 1 hour at room temperature. Immunoreactive proteins were detected using the enhanced chemiluminescence method and autoradiography carried out by exposure to X-ray film.

In vitro proliferation assays

Exponentially growing cell lines were plated into two 96-well plates and incubated overnight at 37°C. Twenty-four hours after plating, 1 plate (D1) was aspirated and stored at −80°C. The other plate (D4) was treated with 10-fold serial dilutions of ridaforolimus (1,000 to 0.0001 nmol/L) or vehicle (ethanol). Following 72 hours culture at 37°C, the plates were aspirated and stored at −80°C for proliferation analysis. The D1 and D4 plates were assessed simultaneously for cell growth using the CyQUANT Cell Proliferation Assay Kit (Invitrogen). Doubling time (DT) = [0.301 × (72)/log(day4/day1)]. Doublings = 72/DT. Cell growth rate (%) = doublings ridaforolimus/doublings vehicle × 100. $I_{max} = 100 -$ cell growth rate (%) at the dose at which maximum inhibition is observed. I_{max} was used to determine the relative sensitivity of each cell line.

Measurement of VEGF production

HT-1080 cells were engineered to constitutively secrete human growth hormone (hGH) by retroviral transduction with the LGH vector to generate the HT-1080/LGH cell line. The LGH vector is a derivative of pLXSN (Clontech) containing the human growth hormone coding region under the control of the retroviral LTR. HT-1080/LGH cells were seeded into 24-well plates and incubated in the presence of increasing concentrations of ridaforolimus (0–100 nmol/L). Media was replaced plus or minus the appropriate drug concentration every 24 hours for 5 days. Levels of VEGF and hGH secreted into the cell culture medium were quantitated using commercial ELISA kits according to manufacturers' instructions (R&D Systems Inc. and Roche Applied Science, respectively). VEGF levels were normalized to hGH levels and expressed as a percentage of normalized VEGF secretion in untreated cells.

Immunosuppression studies

All animal research protocols were carried out in accordance with the guidelines of the American Association of Laboratory Animal Care. Female C57bl/6 and BALB/c mice, 5 to 6 weeks of age, were received from Charles River Laboratories. C57bl/6 mice received Balb/c skin allografts on their backs and were randomized into 7 groups of 10 animals. Ridaforolimus or vehicle was administered subcutaneously, in the rear haunch area, to avoid inadvertent disruption of the grafted skin. A control group was administered vehicle once daily. The remaining 6 groups received ridaforolimus at 3 or 10 mg/kg, either daily, 5 continuous days every other week, or once weekly. Administration of vehicle or ridaforolimus was initiated on the day of skin-graft transplantation. All animals were dosed until full rejection of their graft (assessed by visual inspection). The duration of skin-graft survival was determined within each

treatment group and was compared with the duration of the skin-graft survival in the vehicle control group.

In vivo growth inhibition studies

Five- to 6-week-old male and female athymic NCr-*nu* mice (Taconic Farms; Charles River Laboratories) were used. Xenografts were established by subcutaneous implantation of 30- to 40-mg fragments of PC-3, A549, HCT-116, MCF7, and PANC-1 tumors in mice near the right axilliary area. Treatment was initiated when tumors reached 75 to 245 mm^3 in size after 8 to 20 days following implantation. Animals selected with tumors in the proper size range were assigned to various treatment groups (10 animals per cohort) so that the median tumor weights on the first day of treatment were as close as possible to each other. Ridaforolimus, at dosages of 3 and 10 mg/kg, was administered i.p. on 2 different treatment schedules: (a) daily, 5 continuous days every other week and (b) once weekly. The control group was untreated. For the sarcoma study, the human leiomyosarcoma cell line SK-LMS-1 was used. Seven-week-old female nude mice (Charles River Laboratories) were used for subcutaneous tumor cell implantation (2×10^6 cells) at the right flank area on the back of each animal. Animals were randomly assigned to individual treatment groups (10 animals per cohort). Ridaforolimus, at dosages of 0.1, 0.3, 1, 3, and 10 mg/kg, was administered by the i.p. route using the daily for 5 days every other week schedule. The control group was treated with vehicle alone.

Mice were monitored daily and weighed twice per week. Tumor size was evaluated twice per week by caliper measurements using the following formula: tumor volume = (length $\times$ width^2)/2. Tumor growth inhibition (TGI) was calculated when the treatment period was finished, TGI = $(1 - \Delta T/\Delta C) \times 100$, where ΔT stands for mean tumor volume change of each treatment group and ΔC for mean tumor volume change of control group. The tumor volume data were collected and analyzed with 1-way ANOVA test (GraphPad PRISM). Each ridaforolimus treatment group was further compared with the vehicle control group for statistical significance using Dunnett's test. A value of $P < 0.05$ was considered to be statistically significant.

Pharmacokinetic and pharmacodynamic studies

The pharmacokinetics of ridaforolimus was determined in female NCr-*nu* nude mice after a single i.p. administration of 0.3, 1, 3, or 10 mg/kg. Ridaforolimus was formulated in a mixed vehicle (dimethyl acetamide/polysorbate 80/polyethylene glycol-400/water 10/10/40/40 (v/v/v/v)) and the formulation was administered at a fixed volume of 8 mL/kg. Blood was collected at 0.25, 0.5, 1, 2, 4, 6, 16, and 24 hours (4 mice/time point). A portion of blood was processed to plasma and ridaforolimus levels in whole blood and plasma were determined by an LC/MS/MS method. PK parameters were calculated using WinNonLin version 5.0.

For pharmacodynamics analysis, when SK-LMS-1 xenograft tumors reached ~500 mm^3 in size cohorts of 3 mice each were administered ridaforolimus i.p. and tumors harvested 6, 24, or 72 hours later. Individual tumors were homogenized in ice-cold radioimmunoprecipitation assay buffer containing protease and phosphatase inhibitors and clarified by centrifugation. Tumor lysates were analyzed by immunoblotting using antibodies against phospho-S6 (S235/236), phospho-4E-BP1 (Ser65/Thr70) and GAPDH. Phospho-S6 and phospho-4E-BP1 levels were normalized to the amount of total GAPDH present in each sample and then expressed as a relative percentage compared with the vehicle treated controls. Ridaforolimus concentrations in plasma were determined at the same time points as described above. Reported concentrations are the mean values from 3 mice/time point/group.

Results

Ridaforolimus inhibits key cellular activities controlled by mTOR

The ability of ridaforolimus to inhibit mTOR activity was initially assessed by determining its effect on phosphorylation of the downstream signaling proteins ribosomal protein S6 and 4E-BP1. Treatment of HT-1080 fibrosarcoma cells with ridaforolimus resulted in a dose-dependent inhibition of phosphorylation of both S6 and 4E-BP1 (Fig. 1A), with 50% of complete inhibition (IC_{50}) achieved at concentrations of 0.2 and 5.6 nmol/L, respectively, and 50% of maximal inhibition (EC_{50}) achieved at concentrations of 0.2 and 1.0 nmol/L, respectively. Whereas ridaforolimus treatment led to a complete inhibition of phosphorylation of S6 in these cells, 4E-BP1 phosphorylation was inhibited by only 54%, possibly reflecting the fact that 4E-BP1 can also be phosphorylated by an mTOR-independent mechanism in some cell lines (29). This difference in effects of ridaforolimus on S6 and 4E-BP1 phosphorylation was also observed in another sarcoma cell line, SK-LMS-1, whereas in MCF-7 cells (breast) near complete inhibition of both S6 and 4E-BP1 phosphorylation was observed (Supplementary Fig. S2). In all cell lines examined, the effects of ridaforolimus on S6 and 4E-BP1 phosphorylation were similar to those observed with rapamycin (Supplementary Fig. S2 and data not shown).

Using a maximally efficacious concentration of ridaforolimus, we next examined its effect on cellular activities known to be regulated by mTOR. Treatment of HT-1080 cells with ridaforolimus led to a decrease in cell size, as reflected by a leftward shift in the mean FSC-H of cells analyzed by flow cytometry (Fig. 1B) and an increase in the proportion of cells in the G_1 phase of the cell cycle, as detected by an increase in the percentage of cells with diploid DNA content (Fig. 1C). As evidenced by the lack of an increase in the sub-G_1 fraction (Fig. 1C), ridaforolimus displayed no significant proapoptotic activity. This finding was confirmed by studies which failed to

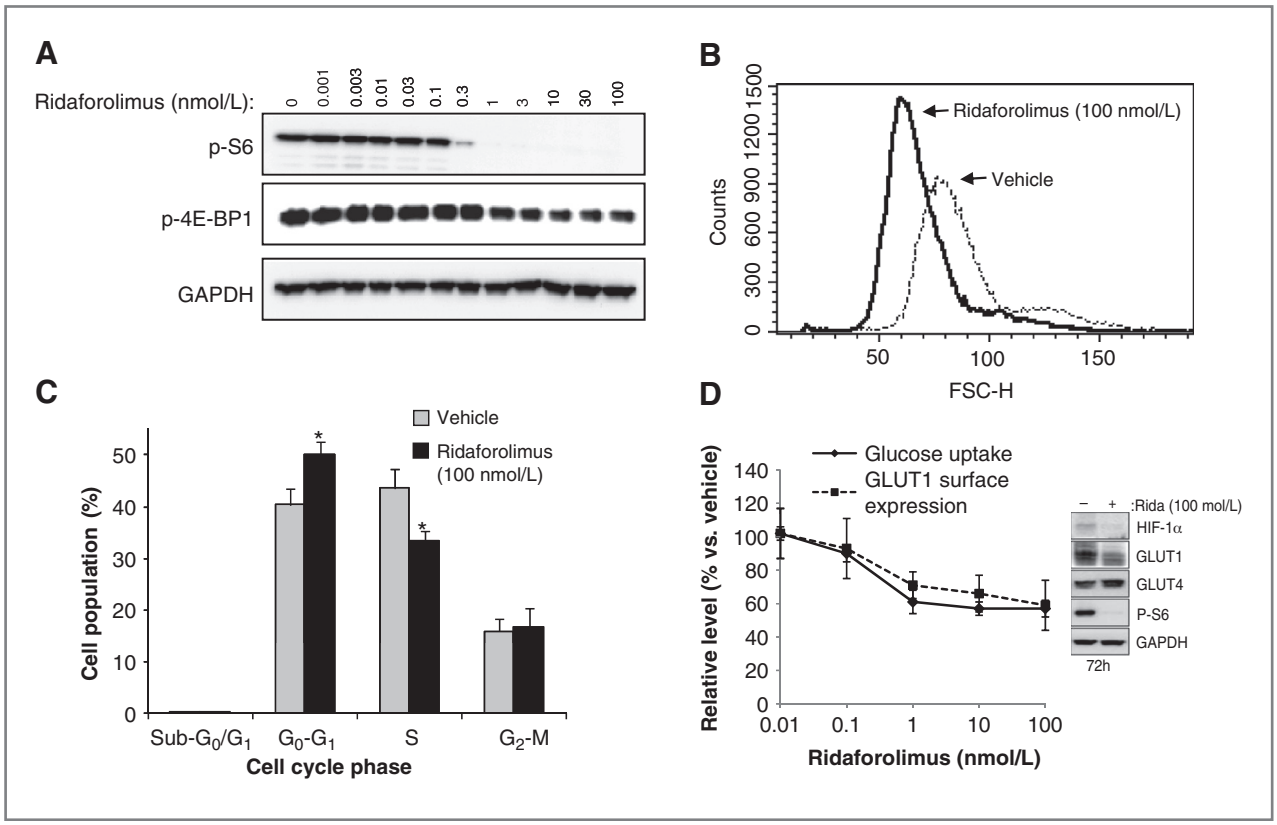

Figure 1. Ridaforolimus attenuates mTOR signaling, resulting in cell shrinkage, cytostatic, and metabolic effects. A, to evaluate target inhibition, HT-1080 cells were treated with increasing concentrations of ridaforolimus for 2 hours before harvest and immunoblotting to assess levels of phosphorylated ribosomal protein S6 (p-S6) and 4E-BP1 (p-4E-BP1). GAPDH was included as a loading control. B, representative FSC-H graph with a plot of HT-1080 cells treated with 100 nmol/L ridaforolimus for 72 hours overlaid with a plot from untreated control cells. Mean FSC-H values for untreated and ridaforolimus-treated cells were 89 and 69, respectively. C, HT-1080 cells were incubated in the presence of 100 nmol/L ridaforolimus or vehicle control for 24 hours. Cells were harvested, stained with propidium iodide, and analyzed by flow cytometry to determine DNA content. The percentage of cells in G_1-, S-, 100 or G_2-M phase was calculated from FL-2 histograms using ModFit Lt software. *, $P < 0.003$. D, HT-1080 cells were treated with vehicle, 0.01, 0.1, 1.0, 10, or 100 nmol/L ridaforolimus for 48 hours. For glucose uptake, cells were exposed for 2 hours to the fluorescent glucose analogue 2-NBDG. The level of uptake of this analogue after 2-hour incubation was determined by FACS as the geometric mean of fluorescence intensity of the cell population for each sample. For GLUT1 surface expression, cells were incubated with enhanced green fluorescent protein-conjugated GLUT1 ligand for 30 minutes and the level of binding determined by FACS as above. The relative percent glucose uptake and GLUT1 expression presented was calculated as the ratio of the geometric means of drug treated versus vehicle treated cells. Inset, HT-1080 cells were treated with 100 nmol/L ridaforolimus for 72 hours and the expression levels of HIF-1α, GLUT1, GLUT4, and p-S6 determined by immunoblot.

detect an increase in caspase 3/7 activity in HT-1080 cells, and other cell lines, treated with ridaforolimus (data not shown). As mTOR has also been implicated in the control of glucose uptake by tumor cells (19, 20), we next evaluated the effects of ridaforolimus on this process. Treatment of HT-1080 cells with ridaforolimus inhibited glucose uptake by 43%, with the half maximal effect achieved between 0.1 and 1 nmol/L, and a parallel decrease in GLUT1 surface expression was observed (Fig. 1D). Both HIF1α and GLUT1 total protein expression were also inhibited by ridaforolimus, whereas levels of the related GLUT4 transporter were unaffected (Fig. 1D, inset). Overall, these data show that ridaforolimus is a potent inhibitor of cell growth, division, and glucose metabolism, all key cellular activities regulated by mTOR.

Ridaforolimus inhibits proliferation of a broad panel of cell lines

We next set out to characterize the effect that ridaforolimus has on proliferation of a broad panel of cell lines and to examine molecular markers that might correlate with the level of sensitivity of cells to ridaforolimus. Because mTOR inhibition can have cytostatic effects (2), particular attention was paid to the assay methodology used to assess the sensitivity of cells to ridaforolimus to ensure compatibility with this potential mechanism. First, the effect of ridaforolimus on the rate of cell proliferation, rather than on absolute cell number, was examined. This readout was selected because the relative effect of a cytostatic drug on cell number is influenced by the normal doubling time of the cells being studied, making valid comparisons

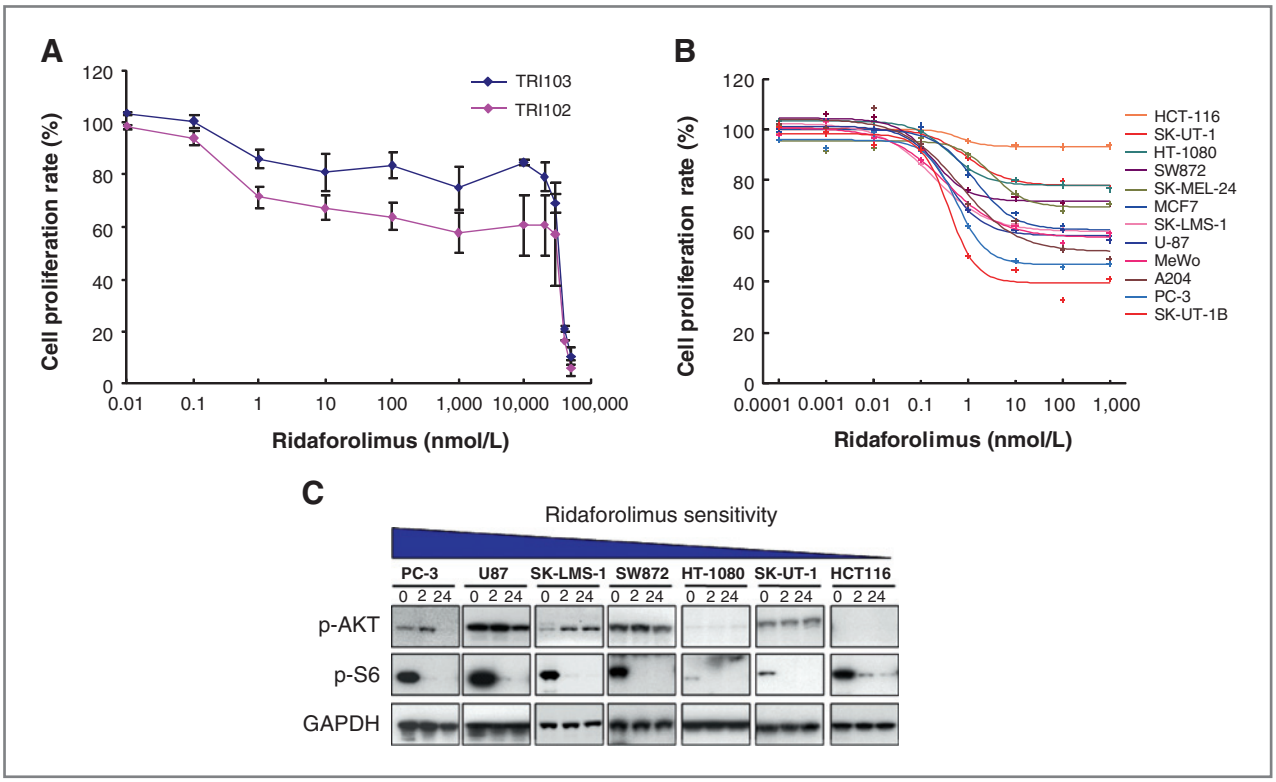

Figure 2. Ridaforolimus treatment inhibits tumor cell proliferation independent of PTEN status or AKT activation. To evaluate the level of sensitivity of cells to ridaforolimus, we measured the effect on the rate of cell proliferation rather than on the absolute cell number, because the effect of a cytostatic drug on absolute cell number is directly influenced by the intrinsic cell doubling time. A, matched isogenic renal angiomyolipoma cell lines, TRI102 and TRI103, were treated with ridaforolimus over a broad dose range (0–100 μmol/L). Points, means from duplicate experiments; bars, SD. B, determination of ridaforolimus sensitivity of a panel of tumor cell lines over the indicated concentration range, harvested 72 hours after drug exposure, as described in Materials and Methods. Plot depicts change in growth rate of ridaforolimus-treated cells compared with the growth of vehicle-treated control cells (% cell growth rate). Points, means from at least 3 experiments. C, expression levels of phosphorylated AKT and ribosomal protein S6 (p-AKT and p-S6, respectively) determined by immunoblot analysis following single administration of ridaforolimus (100 nmol/L) for 2 or 24 hours. Phospho-S6 levels were included to confirm target inhibition over the 24-hour time course.

between cell lines difficult (i.e., during a defined assay period, a cytostatic drug will appear to have a greater effect on proliferation of cells that double more quickly in the absence of drug than those that double more slowly). Second, an assay that measures DNA content was used to enumerate cells, rather than one that measures metabolic activity, to avoid potential confounding effects that mTOR inhibition might have on metabolic readouts. Finally, 2 separate parameters were measured to assess the sensitivity of cell lines: the maximal inhibitory effect ridaforolimus had on the cell proliferation rate (i.e., the I_{max}) and the concentration of ridaforolimus that induced half the maximal effect (i.e., the EC_{50}). Because treatment with a cytostatic compound often does not result in 50% growth inhibition (IC_{50}), IC_{50} values may not be calculated for many cell lines.

In an initial study, the effect of a broad range of ridaforolimus concentrations (0.01–100,000 nmol/L) on cell proliferation was examined using a pair of isogenic cell lines that differ only in the activation state of the mTOR pathway. TRI102 cells have a hyperactivated mTOR pathway by virtue of being null for TSC2; in TRI103 cells normal mTOR pathway regulation has been restored by stable reintroduction of the *TSC2* gene (14). In the submicromolar concentration range ridaforolimus treatment had a cytostatic effect on both cell lines. However, a greater I_{max} was seen in the cells with a constitutively activated mTOR pathway (TRI102, Fig. 2A). Despite the difference in the I_{max} achieved over this range, the EC_{50} was similar for both lines, ~1 nmol/L. In a concentration range more than 4 orders of magnitude higher (i.e., >30,000 nmol/L), ridaforolimus induced an equivalently potent cytotoxic effect on both cell lines, suggesting that this effect was independent of mTOR. Thus, to restrict analysis of activities of ridaforolimus to those dependent on mTOR inhibition subsequent studies were carried out using only submicromolar concentrations. In this concentration range, these results suggest that the activation status of the mTOR pathway could potentially impact cellular responsiveness to the drug, at least in an otherwise isogenic system. Furthermore, these studies support the

Table 1. Maximal inhibition (I_{max}) values, EC_{50} determination, and PTEN status of the panel of cell lines shown in Fig. 2B

Line	Cancer type	I_{max} (%)	EC_{50}, nmol/L	PTEN
HCT-116	Colon	7	0.6	+
SK-UT-1	Leiomyosarcoma	22	1.0	−
HT-1080	Fibrosarcoma	22	0.5	+
SW872	Liposarcoma	28	0.2	−
SK-MEL-24	Melanoma	30	2.3	−
MCF7	Breast	39	1.3	+
SK-LMS-1	Leiomyosarcoma	40	0.2	+
U-87	Glioblastoma	41	0.4	−
MeWo	Melanoma	42	0.3	+
A204	Rhabdomyosarcoma	47	0.8	+
PC 3	Prostate	53	0 5	−
SK-UT-1B	Endometrial	61	0.4	−

use of the I_{max} parameter as a differentiator of the effects of ridaforolimus on different cell lines.

The antiproliferative activity of ridaforolimus was next assessed against a panel of 12 additional cell lines representing a variety of tumor types. Exposure to ridaforolimus reduced the proliferation of all cell lines, with a broad range of sensitivities observed (Fig. 2B). HCT-116 cells were the least sensitive, with an I_{max} of only 7%, whereas SK-UT-1B cells were the most sensitive, with an I_{max} of 61% (Table 1). Despite the range of sensitivities, the EC_{50} values for all cell lines were similar, all being in the range of 1 nmol/L (Table 1). Notably, in HT-1080 cells, the EC_{50} for inhibition of cell proliferation (0.5 nmol/L) was similar to the EC_{50s} for inhibition of S6 and 4E-BP1 phosphorylation (Fig. 1A). These results suggest that the cytostatic effects observed in these cell lines are mediated by mTOR inhibition and that the magnitude of the effect (I_{max}) is driven by intrinsic properties of each cell line.

PTEN and AKT phosphorylation status does not predict response to ridaforolimus in a heterogeneous cell line panel

To begin to explore potential molecular correlates of sensitivity, we assessed the relationship between PTEN status and the degree of inhibition by ridaforolimus. As a negative regulator of the mTOR pathway, loss of PTEN has been suggested to confer sensitivity to mTOR inhibitors (8, 9). As shown in Table 1, the presence or absence of PTEN did not appear to correlate with the sensitivity of cells to ridaforolimus as there were PTEN positive and negative cell lines at all levels of sensitivity. Thus, it appears that loss of PTEN expression alone is not a strong predictor of sensitivity to ridaforolimus, at least in a heterogeneous panel of cell lines.

Inhibition of mTOR has been shown to induce AKT phosphorylation and activation through inhibition of a negative feedback loop, at least in a subset of cell lines (30, 31). We examined the effect of ridaforolimus on AKT phosphorylation in 7 cell lines that have a range of sensitivities to ridaforolimus. As shown in Fig. 2C, baseline levels of phosphorylated AKT and the effect that ridaforolimus had on AKT phosphorylation after exposure for 2 and 24 hours varied across the cell lines but neither parameter associated with the level of sensitivity of a cell line to ridaforolimus. However, the temporal activation of AKT in some of the lines (e.g., PC-3 and SK-LMS-1) suggests that ridaforolimus is selectively targeting mTORC1 and not mTORC2 complexes, consistent with the action of other members of the rapamycin analogue class of therapeutic agents. As expected, inhibition of S6 phosphorylation was rapid and sustained in all cell lines (Fig. 2C).

Ridaforolimus displays antiangiogenic properties

We next conducted studies to investigate potential antiangiogenic effects of ridaforolimus, including its effect on production of VEGF and on the proliferation of endothelial cells, activities previously shown to be regulated by mTOR (23, 32). The effect of ridaforolimus on production of VEGF was assessed by treating HT-1080 cells, which secrete VEGF constitutively, with 100 nmol/L ridaforolimus. To control for other activities of ridaforolimus, including its general effects on protein translation and cell proliferation, a derivative of the HT-1080 cell line was engineered that constitutively secretes hGH, to allow levels of secreted VEGF to be normalized to levels of secreted hGH. As shown in Fig. 3A, ridaforolimus potently and selectively inhibited VEGF production in a dose-dependent manner, with an EC_{50} of approximately 0.1 nmol/L. This effect was selective for VEGF, as it was apparent even after normalization to hGH levels. In a second study, ridaforolimus was shown to potently inhibit proliferation of human endothelial cells (Fig. 3B) with an EC_{50} of 0.1 nmol/L and with an I_{max} of 63%, which was greater than the I_{max} of all tumor cell lines examined (Table 1). These results suggest that ridaforolimus may have antiangiogenic activities *in vivo*.

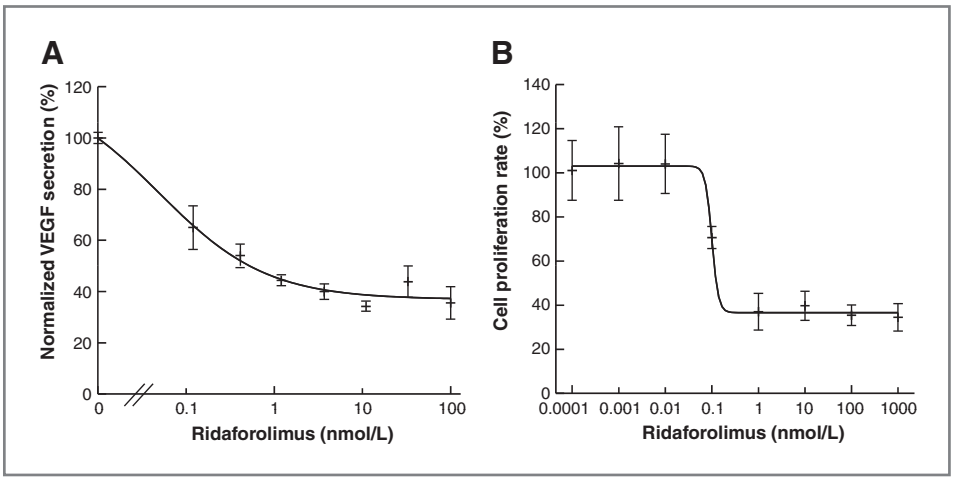

Figure 3. Ridaforolimus inhibits VEGF production and endothelial cell proliferation. A, HT-1080 cells engineered to stably express hGH were incubated in the presence or absence of ridaforolimus at the indicated concentrations for 5 days. Medium (plus or minus drug) was replaced every 24 hours. VEGF and hGH levels in the culture medium were measured using ELISA as described in Materials and Methods. Plot shows VEGF levels normalized to hGH levels and expressed as a percentage of VEGF secreted relative to untreated cells. B, determination of ridaforolimus sensitivity of HUVEC cells over the indicated concentration range, harvested 72 hours after drug exposure. Plot depicts change in growth rate of ridaforolimus-treated cells compared with the growth of vehicle-treated control cells (% cell growth rate). Points, means from 3 experiments; bars, SD.

Intermittent dosing of ridaforolimus reduces immunosuppressive activity *in vivo*

To effectively study the antitumor effects of ridaforolimus in *in vivo* models, we were interested in determining optimal dosing regimens. The mTOR inhibitor rapamycin, administered on a daily schedule, is used clinically as an immunosuppressive agent to prevent allograft rejection (33). Although the potential impact of this activity on antitumor uses of mTOR inhibitors is unclear, we set out to investigate whether intermittent dosing regimens of ridaforolimus might reduce any immunosuppressive effects while preserving antitumor activity. To explore this possibility, we used a mouse skin-allograft rejection model, in which an allografted mouse is dosed with various drug regimens, and the duration of survival of the allograft provides a measure of the immunosuppressive activity of the treatment. Mice bearing allografts were dosed subcutaneously with 3 or 10 mg/kg ridaforolimus on 1 of 3 schedules: daily, 5 continuous days every other week, or once weekly. In mice dosed with vehicle the median survival time for the foreign skin graft was 12 days (Table 2). In mice dosed daily with 10 mg/kg ridaforolimus, the median survival time was extended to 16 days ($P < 0.01$), showing that a daily dosing regimen has an immunosuppressive effect in this model. In contrast, in mice dosed with 10 mg/kg on either of the intermittent dosing regimens graft survival was not significantly extended; the median survival for the daily for 5 days every other week regimen was 13 days ($P > 0.05$) and for the weekly regimen was 12 days ($P > 0.05$). Similar results were observed in mice dosed with 3 mg/kg on the different regimens (Table 2) and similar trends were observed when the mean days of complete graft rejection were compared (data not shown). These results show that in this model, intermittent administration of ridaforolimus limits the immunosuppressive activity that results from daily administration of drug.

Antitumor efficacy and pharmacodynamic activity of ridaforolimus in human tumor xenografts

To determine whether ridaforolimus could exert antitumor effects *in vivo* when delivered using intermittent dosing regimens, mice bearing PC-3 (prostate), HCT-116 (colon), MCF7 (breast), PANC-1 (pancreas), or A549 (lung) xenografts were dosed i.p. with 3 or 10 mg/kg ridaforolimus on 1 of 2 schedules: daily for 5 days every other week or once weekly. The degree to which tumor growth was inhibited, relative to vehicle treated mice, was calculated for each regimen. Tumor growth inhibition was

Table 2. Immunosuppressive effects of ridaforolimus dosage in a mouse skin allograft model

Ridaforolimus schedule	Skin-graft median survival (days)	*P* value
Vehicle	12	N/A
10 mg/kg, daily	16	<0.01[a]
10 mg/kg, QDx5, every other week	13	>0.05
10 mg/kg, weekly	12	>0.05
3 mg/kg, daily	14	<0.01[a]
3 mg/kg, QDx5, every other week	12	>0.05
3 mg/kg, weekly	11	>0.05

Abbreviation: QDx5, daily for 5 days.
[a]Statistical significance.

Table 3. Efficacy of daily for 5 days every other week and weekly dosing schedules in multiple human tumor xenograft models

Xenograft model	Dosing regimen	Tumor growth inhibition (%)	
		3 mg/kg	10 mg/kg
PC-3	QDx5, every other week	67[a]	83[a]
	Weekly	29	45
HCT-116	QDx5, every other week	48[a]	63[a]
	Weekly	2	0
MCF7	QDx5, every other week	50[a]	61[a]
	Weekly	25	43[b]
PANC-1	QDx5, every other week	54[a]	65[a]
	Weekly	37[b]	15
A549	QDx5, every other week	42	40
	Weekly	51[b]	63[a]

Abbreviation: QDx5, daily for 5 days.
[a]$P < 0.01$.
[b]$P < 0.05$.

observed in all 5 models (Table 3; Supplementary Fig. S3). The degree and pattern of tumor growth inhibition was particularly notable when mice were dosed on the daily for 5 days every other week regimen. In 4 of the 5 models, significant inhibition was observed when mice were dosed with 3 mg/kg on the daily for 5 days every other week schedule (15 mg/kg over 2 weeks), whereas when mice were dosed with 10 mg/kg on a once weekly schedule (20 mg/kg over 2 weeks) significant inhibition was only seen in 1 model. Dosing on the daily for 5 days every other week schedule also revealed a general trend of enhanced tumor growth inhibition during the 5 day dosing period compared with 9-day period between doses (Supplementary Fig. S3).

To further explore the efficacy of the daily for 5 days every other week dosing schedule, mice bearing SK-LMS-1 cell-derived xenografts (sarcoma) were treated i.p. with doses ranging from 0.1 to 10 mg/kg. As shown in Fig. 4A, ridaforolimus inhibited tumor growth in a dose-dependent manner, with 0.3 mg/kg being the lowest dose that inhibited tumor growth significantly and 3 and 10 mg/kg doses achieving maximum inhibition.

In a separate study, the pharmacokinetic parameters of ridaforolimus were determined in mice administered a single 0.3 to 10 mg/kg dose i.p. A dose-related increase in exposure was observed (Supplementary Table S1). After administration of 1 mg/kg, a dose level shown to be efficacious (Fig. 4A), area under the curves (AUC) of 4,304 and 7,338 h ng/mL were observed in blood and plasma, respectively. After administration of 3 mg/kg, a dose level shown to be maximally efficacious, AUCs of 8,668 and 18,471 h ng/mL were observed. The relatively short *in vivo* half-life of ridaforolimus in blood and plasma (~4 hours) suggests that daily dosing should not result in significant drug accumulation. Therefore, it is reasonable to extrapolate from this single-dose PK study to draw conclusions about multidose pharmacodynamic and efficacy studies.

Finally, we used the SK-LMS-1 xenograft model to determine whether administration of ridaforolimus inhibited mTOR signaling *in vivo* and whether the effect on mTOR signaling was associated with inhibition of tumor growth. In addition, plasma levels of ridaforolimus were measured to examine the relationship between ridaforolimus levels at individual time points and inhibition of mTOR signaling in the tumor. Mice were dosed i.p. for 5 consecutive days with 0.1, 1, or 10 mg/kg ridaforolimus and then tumors and blood were collected at various times after the last dose (6, 24, and 72 hours).

When mice were dosed with 0.1 mg/kg, a dose that did not significantly inhibit tumor growth (Fig. 4A), S6 phosphorylation was only partially inhibited (by 9%–63%) at all 3 postdose time points (Figs. 4B and C). In contrast, when mice were dosed with 1 or 10 mg/kg, doses that significantly inhibited tumor growth (Fig. 4A), S6 phosphorylation was inhibited by more than 95% 6 and 24 hours after dosing. At the 72-hour time point, S6 phosphorylation was still inhibited by more than 95% after administration of 10 mg/kg and by 88% after administration of 1 mg/kg. Consistent with the *in vitro* results showing that 4E-BP1 phosphorylation is not entirely dependent on mTOR in this cell line (Fig. 1A), less pronounced effects were seen on levels of phosphorylated 4E-BP1 although a similar trend was observed (Fig. 4B and D). Although limited sampling precluded a formal assessment of the pharmacokinetic/pharmacodynamic relationship, an association between ridaforolimus plasma levels and pharmacodynamic effect in the tumor could still be observed (Fig. 4C). For example, at the lowest plasma concentrations measured, 2.8 and 9.4 ng/mL, a substantial decrease in S6 phosphorylation (56% and 88%, respectively) was still observed.

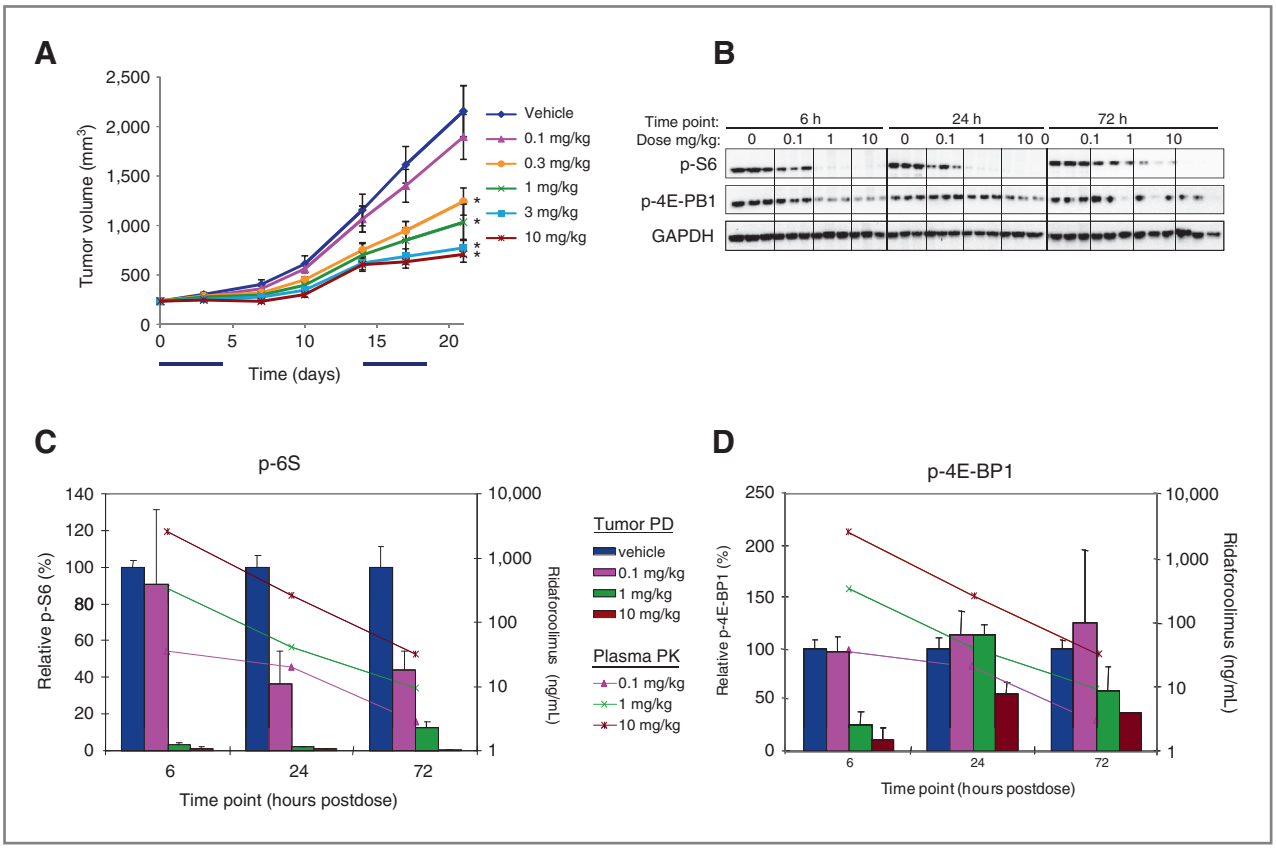

Figure 4. *In vivo* activity and efficacy of ridaforolimus. A, tumor growth inhibition of sarcoma xenografts. Female nude mice bearing established (200 mm^3) SK-LMS-1 human sarcoma xenografts were dosed intraperitoneally with either vehicle or ridaforolimus at a range of doses indicated. The timing of drug administration (5 continuous days every other week) is indicated by the blue horizontal bars. Points, mean tumor volume (mm^3) of 10 mice; bars, SE; *, $P < 0.01$, between control and ridaforolimus treatment groups. B, pharmacodynamic responses following administration of ridaforolimus (0.1, 1, 10 mg/kg) to SK-LMS-1 xenografts. Mice were dosed for 5 consecutive days and tumors then harvested at 6, 24, and 72 hours following the last dose. Data indicate comparative levels of p-S6 and p-4E-BP1 (by immunoblot); GAPDH was included as a loading control. Each lane represents a separate individual xenograft. C, phospho-S6 levels were normalized to the amount of total GAPDH present in each sample and then expressed as a relative percentage compared with the vehicle-treated controls (left axis). Means and SE values of 3 mice per group are plotted. Ridaforolimus concentrations in plasma were determined at the same time points. Reported concentrations are the mean values from 3 mice/group/time point in ng/mL (right axis). D, phospho-4E-BP1 levels were normalized to the amount of total GAPDH present in each sample and then expressed as a relative percentage compared with the vehicle treated controls (left axis). Means and SE values of 3 mice per group are plotted. Ridaforolimus plasma concentrations are as reported in C.

Discussion

Advances in our understanding of the signal transduction pathways that drive oncogenic transformation have resulted in the emergence of rationally designed cancer therapeutics, offering significant promise for improved patient treatment. Rapamycin and its analogues (ridaforolimus, temsirolimus, and everolimus) represent 1 such class of therapeutic agents under clinical investigation in a number of human cancers (34). These compounds target mTOR, a key regulator of protein translation and cell checkpoint control. mTOR also provides a convergence point for multiple signaling pathways that respond to growth factors and nutritional status (1, 2). Ridaforolimus is a novel rapamycin analogue that selectively and potently inhibits mTOR function and, importantly, has shown clinical promise in early trials (27, 28). This report documents the preclinical characterization and mechanistic analysis of the antineoplastic activity displayed by this targeted therapeutic.

Our *in vitro* studies confirmed that ridaforolimus leads to inhibition of mTOR activity and hence to inhibition of tumor cell proliferation. In agreement with previous reports of the generally cytostatic nature of mTOR inhibitors (17, 18), we found that ridaforolimus arrests cell growth without evidence of cell death or apoptosis. Inhibiting mTOR leads to accumulation of cells in the G_1 phase of the cell cycle, in part through blockade of the 4E-BP1/eIF4E signaling which is required for the translation of cell-cycle regulators (12, 13). Consistent with this, we showed a ridaforolimus-dependent increase in the proportion of cells in the G_1 phase. In addition to cell-cycle control, mTOR signaling is a key regulator of cell size (35). Ridaforolimus also inhibited this function, with treatment of HT-1080 cells resulting in a 20% decrease in overall cell size. These cellular effects translated into a

broad antiproliferative activity displayed by ridaforolimus in a variety of human cancer cell lines. The extent of maximal inhibition varied among lines tested suggesting that intrinsic properties of each line determine the magnitude of response. Additional factors such as energy deprivation and nutritional status are also important mediators of mTOR activity; therefore changes in these pathways that accompany malignant transformation are also likely to contribute to the cellular response to mTOR inhibition. Indeed, cancer cells characteristically display abnormally elevated glycolytic activity and we observed that ridaforolimus inhibited glucose uptake in tumor cells. Thus, it is reasonable to suggest that the inhibitory effects both on cell-cycle progression and nutrient utilization underlie the antitumorigenic activity of ridaforolimus.

An important aspect to the clinical development of any targeted therapeutic is the identification of biomarkers that may predict tumor sensitivity to the drug. Early evidence suggested that rapamycin and its analogues might be particularly effective against tumors with PTEN inactivation (9). Loss-of-function mutations in the tumor suppressor gene *PTEN* result in constitutive activation of AKT and upregulation of mTOR activity, and occur with high frequency in a broad range of human malignancies (36). Moreover, studies using isogenic tumor models have shown that loss of PTEN resulted in increased sensitivity to mTOR inhibitors (8, 37). However, we found no correlation between the antiproliferative effects of ridaforolimus and PTEN status in a heterogeneous population of human cancer lines. Similar findings have been reported for everolimus, where PTEN status was insufficient to predict sensitivity in a glioblastoma xenograft model (38). Further, in breast cancer cell lines, Noh and colleagues reported that overexpression of phosphorylated AKT, independent of PTEN status, was associated with rapamycin sensitivity (39). Interestingly, mTOR inhibition itself has been shown to induce AKT phosphorylation and activation through inhibition of a negative feedback loop, at least in a subset of cell lines (30, 31). Such an effect would be expected to attenuate tumor responses. We investigated this possibility but found that induction of AKT phosphorylation following ridaforolimus treatment was also not predictive of the degree of antiproliferative response *in vitro*. This result is consistent with the lack of correlation between everolimus sensitivity and p-AKT induction in a diverse panel of tumor cell lines (40). Although these data suggest that PTEN or AKT do not predict response to ridaforolimus, the heterogeneous nature and small number of cell lines examined preclude definitive assessment of these markers. Alternatively in TSC cell lines, activation of the mTOR pathway by loss of the upstream tumor suppressor, TSC2, did increase sensitivity to ridaforolimus (Fig. 2A). The utility of TSC2 status as a general predictive indicator of mTOR inhibitor activity in cancer remains uncertain. To date, no robust molecular markers predictive of response to an mTOR inhibitor have been determined and clinically validated, and this remains an important challenge in the field.

Added complexity arises from the observation that even cell lines that are poorly sensitive to mTOR inhibitors *in vitro* can be inhibited *in vivo* (41). For example, we found that the *in vitro* sensitivity of HCT-116 cells to ridaforolimus did not predict its *in vivo* sensitivity. HCT-116 cells were the least sensitive to the antiproliferative effects of ridaforolimus *in vitro*, with an I_{max} value of only 7%, yet growth of xenograft tumors was significantly inhibited (48%–63%). It has been proposed that such a discrepancy can be explained, at least in part, through specific antiangiogenic and antivascular activities of mTOR inhibition that manifest *in vivo* (23, 42). HIF-1 transcriptional activation of the *VEGF* gene is a known downstream effect of mTOR signaling, and mTOR inhibitors have been shown to attenuate the expression of both HIF-1 and VEGF (43–45). Here we show significant inhibition of VEGF production in response to ridaforolimus treatment using fibrosarcoma cells that typically secrete substantial levels of this growth factor, as well as potent inhibition of HUVEC cell proliferation. Taken together, these data are consistent with an integral role for mTOR signaling in regulating aspects of endothelial cell biology and angiogenesis, which in turn may influence tumor sensitivity to ridaforolimus.

Because mTOR is ubiquitously expressed and involved in many normal cellular processes, an important consideration for the development of mTOR inhibitors for oncology has been the potential for mechanism-based side effects (46). One known function for mTOR is in controlling immune responses through its role in IL-2–stimulated T cell proliferation. Daily administration of rapamycin is indicated for the prevention of allograft rejection in patients, and rapamycin analogues with similar mTOR inhibitory activity, such as ridaforolimus, would be expected therefore to have similar immunosuppressive potential, which *a priori* would seem to be undesirable in cancer patients. Previous studies have suggested that the effects of mTOR inhibitors on T cells resolve within 24 hours of dosing, suggesting that daily dosing is required to maintain immunosuppression (47). Our studies using a mouse skin allograft rejection assay showed that intermittent administration of ridaforolimus, such as with weekly or daily for 5 days every other week schedules, functionally eliminated the immunosuppressive activity that resulted from daily administration of the drug. However, these identical intermittent schedules and dose levels led to strong antitumor responses in multiple xenograft models. Together, these observations indicate that the antitumor activity of mTOR inhibitors can be uncoupled from their immunosuppressive effects—and potentially from other systemic effects—by using an optimized intermittent dosing regimen.

In xenograft studies, treatment for 5 continuous days every other week was generally superior to the weekly administration regimen. We used this optimized dosing schedule in a sarcoma model to confirm the

association between inhibition of mTOR signaling and inhibition of tumor growth. Doses that inhibited tumor growth significantly (1 or 10 mg/kg) inhibited tumor S6 phosphorylation, whereas a dose that did not inhibit tumor growth significantly (0.1 mg/kg) did not inhibit signaling appreciably. This study also showed that inhibition of S6 phosphorylation could be maintained for at least 72 hours after dosing, which recapitulates the longest period without dosing in a daily for 5 days every week regimen. This finding may help explain why intermittent dosing regimens retain antitumor activity in these models.

The findings reported here have been incorporated into the ongoing clinical development of ridaforolimus, where intermittent dosing schedules, administered intravenously, were well tolerated and shown initial activity in several tumor types, including sarcoma (27, 28). In a phase 1 study that examined the same daily for 5 days regimen explored here (28) levels of exposure in patients administered the recommended phase 2 dose (RP2D) level of 12.5 mg/day (AUC 4,690 ng h/mL in blood) were comparable to those observed after administration of an efficacious dose level of 1 mg/kg in mice (AUC 4,304 h ng/mL in blood). Direct comparison of pharmacokinetic parameters is complicated by differences in blood-plasma partitioning between the species, and a much longer half-life in humans (56–74 hours; ref. 28).

In summary, here we report the preclinical characterization of ridaforolimus, a potent inhibitor of mTOR. Ridaforolimus showed broad inhibitory effects on cell growth, division, metabolism, and angiogenesis, and exhibited antitumor activity in a wide range of *in vitro* and *in vivo* model systems. The relationship between ridaforolimus exposure and activity was established in a broad range of tumor types, as was the relationship between target inhibition and efficacy using a model of sarcoma. Our studies provide strong support for the continued clinical development of ridaforolimus as a targeted cancer therapeutic.

Disclosure of Potential Conflicts of Interest

All authors are present or former employees of ARIAD Pharmaceuticals, Inc. All authors except L. Berk and R. Pollock have ownership interest in ARIAD Pharmaceuticals, Inc.

Acknowledgments

The authors thank Michelle Cookson, Matthew Wong, and Noel Reid for their excellent technical assistance. The authors also thank Richard Bates who provided drafts and editorial assistance during preparation of this manuscript.

The costs of publication of this article were defrayed in part by the payment of page charges. This article must therefore be hereby marked *advertisement* in accordance with 18 U.S.C. Section 1734 solely to indicate this fact.

Received August 24, 2010; revised March 14, 2011; accepted March 29, 2011; published OnlineFirst April 11, 2011.

References

1. Hay N, Sonenberg N. Upstream and downstream of mTOR. Genes Dev 2004;18:1926–45.
2. Bjornsti MA, Houghton PJ. The TOR pathway: a target for cancer therapy. Nat Rev Cancer 2004;4:335–48.
3. Guertin DA, Sabatini DM. An expanding role for mTOR in cancer. Trends Mol Med 2005;11:353–61.
4. Abraham RT, Wiederrecht GJ. Immunopharmacology of rapamycin. Annu Rev Immunol 1996;14:483–510.
5. Hay N. The Akt-mTOR tango and its relevance to cancer. Cancer Cell 2005;8:179–83.
6. Shaw RJ, Cantley LC. Ras, PI(3)K and mTOR signalling controls tumour cell growth. Nature 2006;441:424–30.
7. Toker A, Yoeli-Lerner M. Akt signaling and cancer: surviving but not moving on. Cancer Res 2006;66:3963–6.
8. Neshat MS, Mellinghoff IK, Tran C, Stiles B, Thomas G, Petersen R, et al. Enhanced sensitivity of PTEN-deficient tumors to inhibition of FRAP/mTOR. Proc Natl Acad Sci U S A 2001;98:10314–9.
9. Mills GB, Lu Y, Kohn EC. Linking molecular therapeutics to molecular diagnostics: inhibition of the FRAP/RAFT/TOR component of the PI3K pathway preferentially blocks PTEN mutant cells *in vitro* and *in vivo*. Proc Natl Acad Sci U S A 2001;98:10031–3.
10. Inoki K, Li Y, Zhu T, Wu J, Guan KL. TSC2 is phosphorylated and inhibited by Akt and suppresses mTOR signalling. Nat Cell Biol 2002;4:648–57.
11. Tee AR, Fingar DC, Manning BD, Kwiatkowski DJ, Cantley LC, Blenis J. Tuberous sclerosis complex-1 and -2 gene products function together to inhibit mammalian target of rapamycin (mTOR)-mediated downstream signaling. Proc Natl Acad Sci U S A 2002;99:13571–627
12. Hashemolhosseini S, Nagamine Y, Morley SJ, Desrivieres S, Mercep L, Ferrari S. Rapamycin inhibition of the G_1 to S transition is mediated by effects on cyclin D1 mRNA and protein stability. J Biol Chem 1998;273:14424–9.
13. Rosenwald IB, Kaspar R, Rousseau D, Gehrke L, Leboulch P, Chen JJ, et al. Eukaryotic translation initiation factor 4E regulates expression of cyclin D1 at transcriptional and posttranscriptional levels. J Biol Chem 1995;270:21176–80.
14. Hong F, Larrea MD, Doughty C, Kwiatkowski DJ, Squillace R, Slingerland JM. mTORraptor binds and activates SGK1 to regulate p27 phosphorylation. Mol Cell 2008;30:701–11.
15. Hosoi H, Dilling MB, Shikata T, Liu LN, Shu L, Ashmun RA, et al. Rapamycin causes poorly reversible inhibition of mTOR and induces p53-independent apoptosis in human rhabdomyosarcoma cells. Cancer Res 1999;59:886–94.
16. Huang S, Liu LN, Hosoi H, Dilling MB, Shikata T, Houghton PJ. p53/p21(CIP1) cooperate in enforcing rapamycin-induced G(1) arrest and determine the cellular response to rapamycin. Cancer Res 2001;61:3373–81.
17. Kunz J, Henriquez R, Schneider U, Deuter-Reinhard M, Movva NR, Hall MN. Target of rapamycin in yeast, TOR2, is an essential phosphatidylinositol kinase homolog required for G_1 progression. Cell 1993;73:585–96.
18. Brown EJ, Albers MW, Shin TB, Ichikawa K, Keith CT, Lane WS, et al. A mammalian protein targeted by G_1-arresting rapamycin-receptor complex. Nature 1994;369:756–8.
19. Hudson CC, Liu M, Chiang GG, Otterness DM, Loomis DC, Kaper F, et al. Regulation of hypoxia-inducible factor 1alpha expression and function by the mammalian target of rapamycin. Mol Cell Biol 2002;22:7004–14.
20. Wieman HL, Wofford JA, Rathmell JC. Cytokine stimulation promotes glucose uptake via phosphatidylinositol-3 kinase/Akt regulation of Glut1 activity and trafficking. Mol Biol Cell 2007;18:1437–46.
21. El-Hashemite N, Walker V, Zhang H, Kwiatkowski DJ. Loss of Tsc1 or Tsc2 induces vascular endothelial growth factor production through mammalian target of rapamycin. Cancer Res 2003;63:5173–728

22. Lee DF, Kuo HP, Chen CT, Hsu JM, Chou CK, Wei Y, et al. IKK beta suppression of TSC1 links inflammation and tumor angiogenesis via the mTOR pathway. Cell 2007;130:440–55.
23. Guba M, von Breitenbuch P, Steinbauer M, Koehl G, Flegel S, Hornung M, et al. Rapamycin inhibits primary and metastatic tumor growth by antiangiogenesis: involvement of vascular endothelial growth factor. Nat Med 2002;8:128–35.
24. Schmelzle T, Hall MN. TOR, a central controller of cell growth. Cell 2000;103:253–62.
25. Mahalingam D, Sankhala K, Mita A, Giles FJ, Mita MM. Targeting the mTOR pathway using deforolimus in cancer therapy. Future Oncol 2009;5:291–303.
26. Metcalf CA, Bohacek R, Rozamus LW, Burns KD, Roses JB, Rivera VM, et al. Structure based design of AP23573, a phosphorus-containing analog of rapamycin for anti-tumor therapy. Proc Amer Assoc Cancer Res 2004;45:2476.
27. Hartford CM, Desai AA, Janisch L, Karrison T, Rivera VM, Berk L, et al. A phase I trial to determine the safety, tolerability, and maximum tolerated dose of deforolimus in patients with advanced malignancies. Clin Cancer Res 2009;15:1428–34.
28. Mita MM, Mita AC, Chu QS, Rowinsky EK, Fetterly GJ, Goldston M, et al. Phase I trial of the novel mammalian target of rapamycin inhibitor deforolimus (AP23573; MK-8669) administered intravenously daily for 5 days every 2 weeks to patients with advanced malignancies. J Clin Oncol 2008;26:361–7.
29. Chen WW, Chan DC, Donald C, Lilly MB, Kraft AS. Pim family kinases enhance tumor growth of prostate cancer cells. Mol Cancer Res 2005;3:443–51.
30. Sun SY, Rosenberg LM, Wang X, Zhou Z, Yue P, Fu H, et al. Activation of Akt and eIF4E survival pathways by rapamycin-mediated mammalian target of rapamycin inhibition. Cancer Res 2005;65:7052–8.
31. O'Reilly KE, Rojo F, She QB, Solit D, Mills GB, Smith D, et al. mTOR inhibition induces upstream receptor tyrosine kinase signaling and activates Akt. Cancer Res 2006;66:1500–8.
32. Seeliger H, Guba M, Kleespies A, Jauch KW, Bruns CJ. Role of mTOR in solid tumor systems: a therapeutical target against primary tumor growth, metastases, and angiogenesis. Cancer Metastasis Rev 2007;26:611–2129
33. Patel JK, Kobashigawa JA. Everolimus: an immunosuppressive agent in transplantation. Expert Opin Pharmacother 2006;7:1347–55.
34. Chan S. Targeting the mammalian target of rapamycin (mTOR): a new approach to treating cancer. Br J Cancer 2004;91:1420–4.
35. Fingar DC, Salama S, Tsou C, Harlow E, Blenis J. Mammalian cell size is controlled by mTOR and its downstream targets S6K1 and 4EBP1/eIF4E. Genes Dev 2002;16:1472–87.
36. Chow LM, Baker SJ. PTEN function in normal and neoplastic growth. Cancer Lett 2006;241:184–96.
37. Podsypanina K, Lee RT, Politis C, Hennessy I, Crane A, Puc J, et al. An inhibitor of mTOR reduces neoplasia and normalizes p70/S6 kinase activity in Pten+/− mice. Proc Natl Acad Sci U S A 2001; 98:10320–5.
38. Yang L, Clarke MJ, Carlson BL, Mladek AC, Schroeder MA, Decker P, et al. PTEN loss does not predict for response to RAD001 (Everolimus) in a glioblastoma orthotopic xenograft test panel. Clin Cancer Res 2008;14:3993–4001.
39. Noh WC, Mondesire WH, Peng J, Jian W, Zhang H, Dong J, et al. Determinants of rapamycin sensitivity in breast cancer cells. Clin Cancer Res 2004;10:1013–23
40. Breuleux M, Klopfenstein M, Stephan C, Doughty CA, Barys L, Maira SM, et al. Increased AKT S473 phosphorylation after mTORC1 inhibition is rictor dependent and does not predict tumor cell response to PI3K/mTOR inhibition. Mol Cancer Ther 2009;8: 742–53.
41. Geoerger B, Kerr K, Tang CB, Fung KM, Powell B, Sutton LN, et al. Antitumor activity of the rapamycin analog CCI-779 in human primitive neuroectodermal tumor/medulloblastoma models as single agent and in combination chemotherapy. Cancer Res 2001; 61:1527–32.
42. Lane HA, Wood JM, McSheehy PM, Allegrini PR, Boulay A, Brueggen J, et al. mTOR inhibitor RAD001 (everolimus) has antiangiogenic/vascular properties distinct from a VEGFR tyrosine kinase inhibitor. Clin Cancer Res 2009;15:1612–22.
43. Wan X, Shen N, Mendoza A, Khanna C, Helman LJ. CCI-779 inhibits rhabdomyosarcoma xenograft growth by an antiangiogenic mechanism linked to the targeting of mTOR/Hif-1alpha/VEGF signaling. Neoplasia 2006;8:394–40130
44. Mabuchi S, Altomare DA, Connolly DC, Klein-Szanto A, Litwin S, Hoelzle MK, et al. RAD001 (Everolimus) delays tumor onset and progression in a transgenic mouse model of ovarian cancer. Cancer Res 2007;67:2408–13.
45. Phung TL, Ziv K, Dabydeen D, Eyiah-Mensah G, Riveros M, Perruzzi C, et al. Pathological angiogenesis is induced by sustained Akt signaling and inhibited by rapamycin. Cancer Cell 2006;10: 159–70.
46. Dancey JE. Inhibitors of the mammalian target of rapamycin. Expert Opin Investig Drugs 2005;14:313–28.
47. Gibbons JJ, Discafani C, Peterson R, Hernandex R, Skotnicki J, Frost P. The effect of CCI-779, a novel macrolide anti-tumor agent, on the growth of human tumor cells *in vitro* and in nude mouse xenografts *in vivo*. Proc Amer Assoc Cancer Res 1999;40:2000.